Analysis of the MODIS Above-Cloud Aerosol Retrieval Algorithm Using MCARS

Galina Wind[1,2], Arlindo M. da Silva[2], Kerry G. Meyer[2], Steven Platnick[2] and Peter M. Norris[3,2]

[1] SSAI, Inc. 10210 Greenbelt Road, Suite 600, Lanham, Maryland 20706, USA

[2] NASA Goddard Space Flight Center, 8800 Greenbelt Rd. Greenbelt, Maryland, 20771, USA

[3] Universities Space Research Association, 7178 Columbia Gateway Dr., Columbia, MD 21046, USA

Correspondence to: G. Wind (Gala.Wind@nasa.gov)

Abstract

The Multi-sensor Cloud and Aerosol Retrieval Simulator (MCARS) presently produces synthetic radiance data from Goddard Earth Observing System version 5 (GEOS-5) model output as if the Moderate Resolution Imaging Spectroradiometer (MODIS) was viewing a combination of atmospheric column inclusive of clouds, aerosols and a variety of gases and land/ocean surface at a specific location. In this paper we use MCARS to study the MODIS Above-Cloud AEROsol retrieval algorithm (MOD06ACAERO). MOD06ACAERO is presently a regional research algorithm able to retrieve aerosol optical thickness over clouds, in particular absorbing biomass burning aerosols overlying marine boundary layer clouds in the Southeastern Atlantic Ocean. The algorithm's ability to provide aerosol information in cloudy conditions makes it a valuable source of information for modeling and climate studies in an area where current clear sky-only operational MODIS aerosol retrievals effectively have a data gap between the months of June and October. We use MCARS for a verification and closure study of the MOD06ACAERO algorithm. The purpose of this study is to develop a set of constraints a model developer might use during assimilation of MOD06ACAERO data.

Our simulations indicate that the MOD06ACAERO algorithm performs well for marine boundary layer clouds in the SE Atlantic provided some specific screening rules are observed. For the present study, a combination of five simulated MODIS data granules was used for a dataset of 13.5 million samples with known input conditions. When pixel retrieval uncertainty was less than 30%, optical thickness of the underlying cloud layer was greater than 4 and scattering angle range within the cloud bow was excluded, MOD06ACAERO retrievals agreed with the underlying ground truth (GEOS-5 cloud and aerosol profiles used to generate the synthetic radiances) with a slope of 0.913, offset of 0.06, and RMSE=0.107. When only near-nadir pixels were considered (view zenith angle within +/-20 degrees) the agreement with source data further improved (0.977, 0.051 and 0.096 respectively). Algorithm closure

38   was examined using a single case out of the five used for verification. For closure, the

39   MOD06ACAERO code was modified to use GEOS-5 temperature and moisture profiles as

40   ancillary. Agreement of MOD06ACAERO retrievals with source data for the closure study

41   had a slope of 0.996 with offset -0.007 and RMSE of 0.097 at pixel uncertainty level of less

42   than 40%, illustrating the benefits of high-quality ancillary atmospheric data for such

43   retrievals.

1 Introduction

The MODerate resolution Imaging Spectroradiometer (MODIS) (Barnes et al., 1998) has proven to be an important sensor for aerosol data assimilation purposes for models such as the Goddard Earth Observing System Model, Version 5 (GEOS-5; Rienecker et al. 2008, Molod et al. 2012). There are two MODIS instruments on board NASA's Earth Observing System (EOS) *Terra* and *Aqua* spacecraft. There is a wide variety of data products available from these instruments for Land, Ocean and Atmosphere disciplines. Atmosphere discipline products include cloud mask, cloud top properties, cloud optical and microphysical properties and atmospheric aerosol properties. The MODIS data product files use a designation of MOD for Terra MODIS and MYD for Aqua MODIS. In this paper for brevity we will use "MOD" to refer to both instruments.

The largest contributor of biomass burning aerosols is Southern Africa (Reid et al, 2009, van der Werf et al, 2010, Chang et al, 2021). Biomass burning occurring from June through October creates thick smoke plumes that extend over the adjacent Atlantic Ocean. Prevailing winds in the area transport the smoke over the Southeast Atlantic Ocean (SEAO) and then as far as the Americas (Swap et al., 1996). The same time period coincides with a near-persistent layer of marine boundary-layer (MBL) stratus cloud that extends for several hundred miles westward from the Namibian coast (Devasthale and Thomas, 2011). The MODIS Dark Target aerosol retrieval algorithm (MOD04) that is used for ocean retrievals operates in clear sky conditions only. MOD04_DT retrievals are not provided for each individual MODIS pixel-level, but rather are performed over a 3x3 or 10x10 set of pixels. Moreover aerosol properties are not retrieved over sun glint regions (Kaufman et al, 1997, Levy et al, 2009, 2013). The SEAO region has both extensive seasonal cloud cover and a significant portion of MODIS

68   granules containing sun glint, leading to equally extensive loss of continuous observations

69   from the area.

70   Figure 1 illustrates these conditions using Terra MODIS data from 2006 through 2013.

71   Panel a) shows the percentage of ocean gridboxes in the SEAO area that had daily mean cloud

72   fraction greater than 50% in the MODIS Daily Level-3 gridded product (Hubanks, et al. 2019)

73   stored at 1x1 degree resolution. Here, the SEAO area is defined the same way as in Meyer et

74   al (2015), specifically between -20 and +20 degrees longitude and +4 to -20 degrees

75   longitude. As much as 60% of all ocean gridboxes have cloud fraction greater than 50% in

76   June (day 152) and only increase to the end of September (day 304). A 1-degree resolution

77   gridbox will contain some clear sky and thus at least some aerosol retrievals are possible. As

78   shown in Figure 1 b), in June between 70-80% of all ocean gridboxes contain some aerosol

79   retrievals, though by September that number drops to between 30-50% year over year.

80   Due to aforementioned limitations of the standard dark-target MODIS aerosol algorithm,

81   a model that assimilates aerosol data from SEAO would have very few aerosol retrievals over

82   the ocean available to it. Most of the transport mechanism in the model would be thus

83   governed by the model physical processes (e.g., advection, sedimentation and wet removal

84   and vertical transport) instead of being constrained by observations.

85   The MOD06ACAERO algorithm (Meyer et al. 2015) fills in the aerosol data gap in

86   SEAO as it is able to perform retrievals of aerosol properties above MBL clouds. The

87   algorithm has been evaluated against observations from the Cloud-Aerosol Lidar and Infrared

88   Pathfinder Satellite Observation (CALIPSO) (Winker et al, 2009), but CALIPSO only

89   provides data at nadir and with a very limited spatial coverage. Recent improvements in

90   CALIPSO version 4 aerosol products (Kim et al, 2018) indicate that the comparisons shown

91   of the MOD06ACAERO algorithm with CALIPSO in Meyer et al (2015) would improve

92   somewhat as significant work had been done to remedy the low bias that CALIPSO retrievals

93   have. However, Kim et al (2018) state that the remaining SEA low bias in CALIPSO

94   retrievals of AOD with respect to AERONET and MODIS makes CALIPSO retrievals

95   somewhat problematic as means of aerosol algorithm evaluation for SEAO area. (e.g., Meyer

96   et al, 2013, 2015, Jethva et al, 2014). Observations collected during the ObseRvations of

97   Aerosols above CLouds and their IntEractionS (ORACLES) (Redemann et al, 2021) are

98   currently being used to evaluate the MOD06ACAERO algorithm. Additional descriptions of

99   ORACLES aerosol data can be found in LeBlanc et al (2020) and Pistone et al (2019).

100   In this study we applied an Observing System Simulation Experiment (OSSE) framework

101   to gain insight on the performance of the MOD06ACAERO algorithm. Rather than using the

102   classic analysis/forecast error metric common in Numerical Weather Prediction OSSE studies

103   (e.g., Hoffman and Atlas 2016) we adopt here a "Retrieval OSSE" perspective where the

104   quality of the retrieval is used as the verification metric (Wind et al. 2013, 2016). A radiative

105   transfer code is applied to the model quantities combined with sensor geometry to simulate

106   how a model scene appears to a specific instrument. A retrieval algorithm designed for that

107   instrument can be executed on the simulated measurements. Physical quantities retrieved by

108   the algorithm can be compared to the known simulation input. The algorithm can be examined

109   for closure over a large spatial domain and thus any areas or conditions that may be

110   problematic for the algorithm could be examined, and the strengths and limitations of the

111   algorithm can be extensively documented.

112   The Multi-sensor Cloud and Aerosol Retrieval Simulator (MCARS) is a tool that

113   combines model output with a radiative transfer code in order to simulate radiances that may

114   be measured by a remote sensing instrument if it were passing over the model fields (Wind et

115   al, 2013, 2016). In this paper, MCARS continues to use the combination of the GEOS-5

116   model, correlated-k models of atmospheric transmittance due to various gaseous absorbers for

117   MODIS channels as per Kratz (1995), inline Rayleigh scattering and the Discrete Ordinate

118   Radiative Transfer (DISORT) code (Stamnes et al. 1988) to simulate MODIS radiances. Two

119   improvements have been made to the MCARS code since last publication. The computational

120   resolution has been increased to 32 streams, up from 16. Additionally, for this study the

121   higher resolution 7 km GEOS-5 Nature Run (G5NR) was used in place of the standard 25 km

122   resolution GEOS-5 output (Gelaro et al. 2015, da Silva et al. 2015, Putman et al. 2015).

123   G5NR is a 2-year global, non-hydrostatic mesoscale model dataset for the period 2005-2006

124   produced with the GEOS-5 Atmospheric GCM. The model run is performed at a horizontal

125   resolution of 7 km using a cubed-sphere horizontal grid with 72 vertical levels, extending up

126   to 0.01 hPa (~ 80 km). In addition to standard meteorological parameters (wind, temperature,

127   moisture, surface pressure), this GCM includes 15 aerosol tracers (dust, sea-salt, sulfate, black

128   and organic carbon), O_3 and CO_2. The GEOS-5 NR is driven by prescribed sea-surface

129   temperature and sea-ice, daily volcanic and biomass burning emissions, as well as high-

130   resolution inventories of anthropogenic sources. A description of the GEOS-5 model

131   configuration used for the Nature Run can be found in Putman et al. (2014), while results

132   from a validation exercise appear in Gelaro et al. (2015) and Castellanos et al. (2019).

133   In a previous study of the MOD04_DT code (Wind et al, 2016), we had the advantage of

134   having simultaneous in situ aerosol property measurements from AErosol RObotic NETwork

135   (AERONET) (Holben et al., 1998). AERONET has very limited data available over ocean,

136   mainly from islands and ship transits. Even in places where AERONET is established, no

137   measurements can be obtained in presence of clouds. Therefore, no ground-based in-situ

138   measurements can be included in our analysis of the MOD06ACAERO product and so the

139   analysis is necessarily limited to verification and closure.

140   In sections that follow we will describe the application of MCARS to study the

141   MOD06ACAERO algorithm. Section 2 very briefly describes the MCARS code and the

142   experiment setup. Section 3 describes the MODIS MOD06ACAERO product of Meyer et al.

143   (2015). Section 4 shows the details of the study and study conclusions. Finally, section 5

144   discusses the next steps in MCARS development.

145   **2   MCARS description**

146   The MCARS code was previously described in detail in Wind et al (2013, 2016).

147   Therefore, only a brief description will be given here. Global aerosol, cloud, surface and

148   atmospheric column fields from the G5NR simulation as described above serve as the starting

149   point for radiance simulations. The GOCART bulk aerosol scheme currently used in the

150   G5NR is used for the simulations reported in this paper, with corresponding optical properties

151   as described in Randles et al. (2017), Hess et al (1998) and references within. The simulation

152   input data was produced in accordance with the methods outlined in Wind et al. (2016). The

153   G5NR model output was split into 1-km subcolumns (MODIS pixel resolution) using the

154   independent column approximation method as described in detail in Wind et al. (2013). Here

155   a brief summary of the model data preparation methodology is given.

156   MODIS pixels for each GEOS-5 gridbox were collected and the same number of pixel-

157   like sub-columns was generated using a statistical model of sub-gridcolumn moisture

158   variability. The sub-column generation used a parameterized probability density function

159   (PDF) of total water content for each model layer and a Gaussian copula to correlate these

160   PDFs in the vertical (Norris et al, 2008, Norris and da Silva 2016a,b).

161   The subcolumns generated in this way were subsequently rearranged, to give horizontal

162   spatial coherence, by using a horizontal Gaussian copula applied to condensed water path.

163   This arrangement had to be applied in order to create spatially coherent cloud-like structures.

164 The subcolumns themselves were not altered in any way during this process. If this step is

165 skipped and the subcolumns are placed randomly within each gridbox the MODIS Cloud

166 Optical and Microphysical Properties (MOD06) product (Platnick et al, 2017) would restore

167 many of the pixels to clear sky unless the initial gridbox had close to 100% cloud fraction

168 (Zhang and Platnick 2011; Pincus et al. 2012). The MOD06 product is a necessary input for

169 MOD06ACAERO and must be produced prior to MOD06ACAERO execution. The need for

170 this subcolumn rearrangement is significantly lessened when G5NR is used because the

171 smaller gridboxes are often close to 100% cloudy especially in MBL regimes, but removing

172 the method from the model preparation step was not practical due to its small impact on

173 execution time and possibility of introducing errors.

174   The layer aerosol properties were obtained using the independent column approximation

175 with the same PDF of total water content as used for clouds. A GEOS-5 aerosol species

176 output file was used in conjunction with aerosol optical properties as in Randles et al. (2017).

177 The aerosol phase functions for each of the 15 species output by GEOS-5 were produced and

178 combined on the fly to create a single bulk set of scattering properties and Legendre

179 coefficients. (Wind et al, 2016)

180   Model parameters such as profiles of temperature, pressure, ozone and water vapor

181 together with layer information about clouds and aerosols are combined with solar and view

182 geometry of the MODIS instrument. Surface information is also a combination of GEOS-5

183 information of surface temperature, snow and sea ice cover and MODIS-derived spectral

184 surface albedo (Moody et al. 2007, 2008). All of these parameters are transferred to the

185 DISORT-5 radiative transfer code and reflectances and radiances in 22 MODIS channels

186 between 470nm and 14.2μm are produced. The default computational resolution of DISORT-

187 5 has also been increased to 32 streams up from 16 used in the two previous studies.

188 Additionally some of the simulations in this study were executed at 64 streams. Final MCARS

189   output is packaged in a format identical to the standard MODIS Level-1B radiometric files

190   and is thus completely transparent to any operational or research-level retrieval algorithm

191   code.

192   These simulations were produced at the NASA Center for Climate Simulations (NCCS)

193   supercomputer. Each complete simulation of a MODIS-like granule requires 5.5 hours of wall

194   clock time on 300 processors. Computational throughput can be increased by limiting the

195   scope of the simulation to fit a particular investigation. For this study, however, we retain the

196   full set of channels needed for both cloud and aerosol research.

197

198   **3   MODIS above-cloud aerosol properties product**

199

200   The MODIS above-cloud aerosol properties product (MOD06ACAERO) (Meyer et al.

201   2015) is a regional algorithm able to simultaneously retrieve MBL cloud optical thickness

202   (COT), cloud effective radius, and aerosol optical depth (AOD) above-cloud in the SEAO

203   region. It uses six MODIS channels (bands 1-5 and 7) having central wavelengths of 0.47,

204   0.55, 0.66, 0.86, 1.24 and 2.1μm. The MOD06ACAERO algorithm takes advantage of the

205   strong biomass burning aerosol absorption gradient in the visible (VIS) to near-infrared (NIR)

206   spectrum that, when the aerosol layer overlies a bright cloud, yields differential attenuation

207   (stronger at shorter wavelengths) of the otherwise nearly spectrally invarient top-of-

208   atmosphere cloud reflectance across the VIS/NIR. Sensitivity to cloud optical thickness is

209   localized in the spectral range between 0.47 and 1.24μm and is directly related to the

210   magnitude of reflectance, while sensitivity to above-cloud aerosol optical depth is related to

211   the spectral slope of the reflectance. The MOD06ACAERO algorithm uses 2.1μm channel for

212   cloud effective radius information. That is also consistent with the principal retrieval

213   contained in the MOD06 product (Platnick, et al, 2017)

214   The MOD06ACAERO retrieval inversion uses an optimal estimation-like approach

215   (Rodgers, 1976) that attempts to minimize the difference (cost function) between the six

216   MODIS reflectance observations and forward-modeled reflectance that is a function of cloud

217   optical thickness, effective radius, and above-cloud AOD. However, rather than in-line

218   radiative transfer calculations, MOD06ACAERO relies on a set of pre-computed lookup

219   tables (LUTs) of coupled cloud and above-cloud aerosol reflectance. These LUTs are

220   generated using the same cloud microphysics models used by MOD06 (Platnick et al, 2017)

221   and the absorbing aerosol model used by MOD04_DT over land surfaces (Levy et al, 2013).

222   Retrievals using a second aerosol property model, one based on field campaign data from

223   SAFARI 2000 (Haywood et al, 2003), are also available in MOD06ACAERO output. While

224   these Haywood et al. model retrievals were recommended in Meyer et al (2015), evaluation

225   during the ORACLES campaign revealed deficiencies at certain scattering angle ranges (K.

226   Meyer, private communication). Thus, for this study we use the MOD06ACAERO results

227   based on the MOD04_DT aerosol models.

228   The MOD06ACAERO retrieval operates at 1km resolution, compared to the 10km and

229   3km MOD04_DT resolutions, and simultaneously provides pixel-level estimates of retrieval

230   uncertainty accounting for known and quantifiable error sources (e.g., radiometry,

231   atmospheric profile errors, cloud and aerosol forward model errors) consistent with the

232   MOD06 cloud product methodology (Platnick et al, 2020). Figure 2 shows an example

233   retrieval result from MOD06ACAERO compared to MOD04_DT standard 10km output. The

234   Terra MODIS granule shown here, from 2006 day 224 at 10:05 UTC, has extensive cloud

235   cover over the ocean, typical for this season. MOD04_DT provides a very limited amount of

236   data, localized to the few areas of clear sky, while MOD06ACAERO fills in the above-cloud

237   area. Shinozuka, et al (2020) suggest that above-cloud aerosol retrievals are similar to

238   adjacent clear-sky retrievals and so clear-sky retrievals could be used as an above-cloud

239 proxy. However conditions shown in Figure 2 are common during the SEAO burning season.

240 There are no clear-sky retrievals of aerosol over most of the area due to near uniform

241 coverage by marine stratus, with cloud fraction approaching 80%. Nearest successful clear-

242 sky retrievals are hundreds of miles away. Therefore an above-cloud aerosol retrieval

243 algorithm such as MOD06ACAERO is very much so necessary.

244   MOD06ACAERO uses National Center for Environmental Prediction (NCEP)

245 atmospheric profile products (Derber et al, 1991) for atmospheric correction. As part of our

246 investigation we will look at impact of discrepancies between NCEP and G5NR on retrieved

247 aerosol properties.

248

249 **4   Analysis**

250

251   To create the data used for the MOD06ACAERO verification study, we examined the

252 G5NR dataset for cases that were similar to conditions commonly encountered during the

253 burning season over SEAO. August 2006 was selected because it was a very active smoke

254 season and a significant amount of MBL clouds were present in the model output. Models

255 often have difficulties forming MBL clouds as higher than usual grid and vertical resolution is

256 needed in order to accurately represent the processes that lead to MBL formation in nature.

257   As real Terra and Aqua overpasses are needed in order to define the sun-satellite

258 geometry for the MCARS simulations, satellite orbital tracks had to be considered. Because

259 orbital gaps are prominent in the MODIS data over the SEAO MBL region, care must be

260 taken in selecting specific days and times having adequate sensor geometry. Technically

261 because MCARS is a simulation, orbital gaps have no meaning. But because of the need of

262 actual sensor geometry to start the simulation, it is most expedient to simply browse available

263 MODIS data for a suitable track. Even though G5NR does not perform any data assimilation,

264   the model code is identical to the standard GEOS-5 model. MCARS normally runs on

265   standard GEOS-5 output. In Wind et al (2013) we showed MCARS as a model output

266   verification tool. It is always very desirable to match date/time/orbit when model performance

267   may be compared to real concurrent sensor measurements. Even though no orbital match is

268   required in this study, a decision was made to not alter the standard MCARS operation in

269   order to avoid accidental introduction of software issues. Five cases were selected under these

270   considerations. Three came from Terra MODIS overpasses and two from Aqua MODIS. The

271   times and dates were as follows. Terra MODIS: 2006 day 224, 10:05 UTC, 2006 day 225

272   09:10 UTC, 2006 day 228 09:40 UTC. Aqua MODIS: 2006 day 224 12:55 UTC and 2006 day

273   226 12:40 UTC. This simulated radiance dataset comprises 13.5 million points where the

274   atmospheric column and surface conditions are explicitly known. MOD06ACAERO retrievals

275   were attempted over those points, but of course that does not mean that each attempt produced

276   a successful aerosol retrieval.

277   Figure 3 a) shows simulated RGB images for the 5 MCARS MODIS granules listed

278   above. Also shown in b) are the same simulated granules where the aerosols have been

279   removed from the radiative transfer simulations. This ability to remove clouds, aerosols or

280   gases from the simulation offers extensive control evaluating the performance of retrieval

281   algorithms and diagnosing algorithm deficiencies.

282   There is a significant similarity between the real Terra MODIS granule of Figure 2 and

283   the simulated granule for the same date and time. The G5NR is a free running model and does

284   not perform any data assimilation, and therefore it is not synoptically locked to the particular

285   day depicted in Figure 2. The apparent similarities between Figures 2 and 3 merely reflect the

286   persistent patterns of MBL clouds and smoke in the region. There is no expectation of a match

287   with any real data in this study. It is not a statement to G5NR performance as in other cases

288   the cloud amount/distribution had no match to any real data. It is merely an interesting

289   coincidence. Some granules were selected to include a significant portion of land surface for a

290   later examination of the MOD04_DT retrievals, repeating the study in Wind et al (2016) in a

291   different region (not reported here).

292   This dataset, both the complete and the clean (aerosol-free) versions, was fed through the

293   standard operational MODIS Data Collection 6 cloud product processing chain to produce

294   cloud mask, MOD06 cloud top and optical properties, and finally the MOD06ACAERO

295   output for each case. Results from all granules were then combined and only retrievals for

296   cloudy pixels were examined. The MOD06ACAERO aerosol retrievals were compared to

297   source aerosol optical depth provided by GEOS-5 (Wind et al, 2016). Figure 4 shows results

298   of this comparison. The only constraint on this comparison was that the algorithm-reported

299   pixel-level retrieval uncertainty had to be less than 40% for panel a) and less than 30% for

300   panel b). One of the motivations of this study was to characterize errors in the

301   MOD06ACAERO algorithm for subsequent aerosol data assimilation into GEOS-5. Pixels

302   with higher uncertainties could be considered in the analysis, but assimilating data where the

303   retrieval error is 50% or greater could negatively impact the assimilated fields. As depicted in

304   Figure 4, filtering retrievals at the reported algorithm uncertainty at 40% is very effective to

305   produce a good match between MOD06ACAERO and the G5NR output variables, with the

306   exception of very low AODs. G5NR uses aerosol models described in detail in Randles et al

307   (2017). It is a set of 15 absorbers, properties of which are a function of column relative

308   humidity. MOD06ACAERO in this study uses the MOD04_DT aerosol models, which are

309   distinct in composition and additionally computed at a constant 80% column relative humidity

310   (Levy et al, 2013). Because G5NR mixes aerosols on-the-fly to create bulk layer properties

311   and MOD06ACAERO has a constant regional mixture, there is a natural source of uncertainty

312   in any comparison of MOD06ACAERO retrievals with G5NR. However the regional mixture

313   of MOD04_DT had been used extensively to train the GOCART model used by both GEOS-5

314   and G5NR. Thus we expect the uncertainty due to aerosol model mismatch to be fairly

315   minimal. Same exact situation of aerosol mixture mismatch exists in real data and is most

316   likely greater than the one existing in this simulation. Detailed comparison of GOCART and

317   MOD04_DT aerosol models for biomass burning aerosols has been performed in Wind et al

318   (2016).

319   Meyer et al. (2015) suggest that additionally MOD06ACAERO retrievals should be

320   screened by retrieved cloud optical thickness and that they should be discarded if COT is less

321   than 4.0. We applied this additional constraint onto the retrieval comparison and the result is

322   shown in Figure 5. Discarding the AOD retrievals when cloud is thin improved the match-up

323   against GEOS-5, but there still appears to be an issue when GEOS-5 AOD is very close to

324   zero.

325   The power of MCARS lies in being able to tightly control simulation parameters. The

326   MOD06ACAERO algorithm appears to run into a difficulty at low source AOD. In order to

327   examine the causes for this discrepancy in more detail, we turn our attention to the clean

328   MCARS case shown in figure 3b) by setting the AOD precisely to zero and examining the

329   retrieval performance in such situation. Ideally MOD06ACAERO should retrieve a zero AOD

330   throughout. With an exception of a narrow range of scattering angles between 135 and 145

331   degrees, which corresponds to the cloud bow direction, the algorithm indeed retrieved AOD

332   that was extremely close to zero. Figure 6 depicts the difference between retrieval and source

333   as a function of scattering angle. Retrievals where MOD06ACAERO matched GEOS-5

334   precisely were discarded for clarity. Within the cloud bow MOD06ACAERO tends to return a

335   small positive AOD of about 0.15.

336   The liquid water phase function is very complex in the cloudbow region and is very

337   difficult to model accurately. That particular region has consistently caused difficulties to the

338   standard MOD06 product retrievals of MBL clouds. Both MOD06 and MOD06ACAERO

339 LUTs are computed at 64 DISORT streams. We performed some investigation of this area by

340 running a special simulation for a single case from Terra 2006 day 224 10:05 UTC. This case

341 was selected because the cloudbow is especially noticeable in both real and simulated data.

342 The simulation was also executed using 64 DISORT streams in order to reduce uncertainties

343 associated with the simulation being performed at half the resolution. In cloudbow region

344 more streams would potentially lead to a better model. Unfortunately the cloudbow persisted.

345 It thus may be the case that 64 streams are not sufficient to properly resolve the cloudbow in

346 either simulation or retrieval. Even higher resolution may be advisable. Increasing

347 computational resolution of MOD06 LUTs is presently considered for the upcoming MODIS

348 Data Collection 7. Depending on the results, same increase may occur for MOD06ACAERO.

349 At this time, for purpose of establishment of assimilation constraints, which is the focus of

350 this study, one might simply exclude the cloud bow scattering angle range from consideration

351 until more is known.

352   Figure 7 shows the results of MOD06ACAERO retrievals from Figure 5 where retrievals

353 within the cloud bow have been discarded. The comparison with source data is further

354 improved and the cluster of MOD06ACAERO retrievals present in Figure 5 when GEOS-5

355 AOD was near zero has disappeared.

356   Often better retrievals can be obtained when less oblique view geometry is considered in

357 real data. Pixel size, longer optical path length and 3D effects from clouds can all make

358 retrievals performed at oblique view angles less optimal. In the case of this study, another

359 consideration for imposition of a view zenith limit is that presently MCARS does not account

360 for pixel size growth at oblique view angles. The number of subcolumns generated does not

361 change with view zenith angle. Therefore, MCARS results when view angle is oblique may

362 not be an accurate measure of algorithm performance as only the effects of optical path length

363 are simulated.

364   The MOD06 cloud product outputs cloud top pressure, temperature and height limited to

365   near nadir in addition to full swath products. The "near nadir" is defined as viewing zenith

366   angle less than 32 degrees (Menzel et al, 2008). Figure 8 shows the MOD06ACAERO

367   retrievals of Figure 7 further limited by view zenith angle of less than 32 degrees. When view

368   zenith angle is limited to 32 degrees the comparison with GEOS-5 source data is again

369   improved. We can now show a slope of 0.866 for retrievals with less than 40% error and

370   0.913 for retrievals with error of less than 30%. Note that even though the data extent had

371   been limited, there are still over 600,000 data points left to be ingested into a model if data

372   assimilation were to be attempted in an area where previously the number of such data points

373   was close to 0.

374   We can constrain the view zenith angle range even further as shown in Figure 9, reducing

375   the threshold to 20 degrees. Whereas the comparison shows all around improvement with

376   slope of 0.931 and 0.977 for retrieval error of less than 40% and 30% respectively, the number

377   of points suitable for assimilation shrinks by half. It is not clear if this dataset size reduction

378   can be justified by the improvement in alignment with the source data.

379   With the 20 degree view angle constraint the algorithm results are very close to source

380   data and we could potentially state that we have closure against source GEOS-5 data even

381   though both MOD06 and MOD06ACAERO run under operational conditions used NCEP

382   GDAS data for atmospheric correction (implying a likely overestimation of the error in these

383   profiles). In order to assess the impact of using these GDAS-based profiles we consider a final

384   experiment where we use MCARS pixel-level input profiles for atmospheric correction. The

385   result is shown in Figure 10. When atmospheric profiles are removed as a source of

386   inconsistency, the agreement with source data improves to a slope of 0.996 with intercept of -

387   0.007 and RMSE of 0.097 for retrievals with less than 40% error and slope of 0.989, intercept

388   of 0.03 and RMSE of 0.085 for retrievals with less than 30% error. Small sample size for

389   retrievals with lower uncertainty is the reason for somewhat lesser agreement with source data

390   for this closure experiment. The remaining source of potential disagreement of

391   MOD06ACAERO retrieval with input GEOS-5 data is the difference between aerosol models

392   used by MCARS and MOD06ACAERO. Cloud models between MOD06ACAERO and

393   MCARS are identical in this study. The MOD06ACAERO model is fixed for the region,

394   while the GEOS-5 aerosols are fully dynamic as per Randles et al (2017). However, it is not

395   practical to change either MCARS or MOD06ACAERO code to use a different aerosol model

396   set, and with the agreement being as good as it presently is. A question might be asked as to

397   whether the difference between aerosol models used by MCARS and MOD06ACAERO

398   would be an additional source of disagreement, especially in the light of results in Wind et al

399   (2016). MCARS has the ability to switch between the GEOS-5 aerosols and those used by

400   MOD06ACAERO and MOD04DT. We tested part of the dataset with identical aerosol

401   models between retrieval and simulation and found there to be no significant impact. One

402   reason for that is simulations in Wind et al (2016) dealt with aerosols located near sources.

403   These aerosols, even though they are same basic type, traveled a significant distance from

404   source and have had a chance to absorb water. Once that happens, there is no difference in the

405   scattering properties between the aerosol model used by MOD04DT and GEOS-5. Part of the

406   reason of this specific dataset selection is to also have the cloud-free land present so that we

407   could repeat the experiment in Wind et al (2016) on a different continent. We expect over

408   land, and thus near sources, we would absolutely see the impact of differences in single

409   scattering albedo.

410

411   **5   Conclusions and future directions**

412   This paper is a direct evolution of work started in Wind et al, (2013) and continued in

413   Wind et al (2016). The Multi-sensor Cloud and Aerosol Retrieval Simulator (MCARS) has

414   now been applied as a verification tool for a research-level algorithm. The algorithm studied

415   was the MODIS above-cloud aerosol properties retrieval algorithm of Meyer et al (2015).

416   MCARS computational resolution has been doubled and for this study the high-resolution

417   (7km) GEOS-5 Nature Run model was utilized. The MCARS code produces radiances and

418   reflectances in a standard MODIS Level 1B format after sending the GEOS-5 data through

419   DISORT-5 radiative transfer code. The output can be directly ingested by any retrieval or

420   analysis code that reads data from the MODIS instrument.

421   We used the MCARS code to perform verification and closure study on the

422   MOD06ACAERO algorithm. In this study we generated a set of five MODIS granules located

423   in the Southeastern Atlantic Ocean off the coast of Namibia. We executed the

424   MOD06ACAERO code on this case set. In the verification part of the study the algorithm

425   performed very well. When pixels with less than 30% uncertainty were considered with

426   underlying cloud layer having optical thickness greater than 4 the algorithm matched the

427   source GEOS-5 aerosol optical depth with slope of 0.774 and offset of 0.076, RMSE = 0.131.

428   On further examination, executing the algorithm on the same case set with aerosols removed it

429   was determined that there might be data that is less useful around the scattering angle of 140

430   degrees, the cloud bow direction. When the cloud bow pixels were excluded the slope

431   improved to 0.913. The near-nadir slope with angle limit of 20 degrees improved the

432   agreement further to 0.977, RMSE=0.096.

433   To look at closure one of the five cases was selected. For closure both MOD06 and

434   MOD06ACAERO codes were modified to use MCARS input profiles as ancillary instead of

435   the NCEP analysis used in operations (Platnick et al, 2017). When the results were compared

436   to source GEOS-5 data a slope of 0.996 with offset of -0.007 and RMSE = 0.097 was reached

437   for pixels with less than 40% uncertainty. The agreement was slightly worse for uncertainties

438   less than 30% (slope 0.989, offset 0.03 and RMSE = 0.085) but that was mainly due to having

439   a smaller number of pixels in the set, only 130,000.

440   The results of this study suggest that retrievals produced by MOD06ACAERO are of

441   good initial quality and would be a valuable addition to model data assimilation streams with

442   the following constraints. MOD06ACAERO pixels should be assimilated if retrieval

443   uncertainly is less than 40%, if optical thickness of the underlying cloud layer is greater than

444   4.0 and if the pixel scattering angle is outside the cloud bow. Additionally, an even tighter

445   constraint can be added to only take pixels that are near nadir.

446   This study is yet another example of the capabilities of the MCARS framework. There

447   are many other potential applications of the MCARS code, including extending the simulator

448   to other sensors and examining the performance of fast retrieval simulators used in climate

449   modeling.

450   **6   Code and Data Availability**

451   The MCARS code is free of charge and can be downloaded here:

452   https://zenodo.org/record/5224964#.YR_DOdNKjaV

453

454

455

Author Contributions

456 **Author Contributions**

457   GW is the development and experiment design lead on the MCARS project. She

458 maintains the code, creates experiments and performs most of the analysis of experiment data.

459   AdS and PN assist with preparation, interpretation and integration of the GEOS-5 model

460 data.

461   KM is the author of MODIS above-cloud aerosol retrieval algorithm, the subject of this

462 simulation experiment. He assisted with interpretation of retrieval results and development of

463 assimilation constraints for the above-cloud aerosol product.

464   SP assisted with analysis, evaluation and interpretation of all experiment data.

465

466 **Acknowledgements**

467   The authors would like to thank Brad Wind for the initial idea for creating a simulator,

468 the output of which could be transparently used with remote sensing retrieval codes.

469

470

References

Barnes, W. L., T. S. Pagano, and V. V. Salomonson, 1998: Prelaunch characteristics of the Moderate Resolution Imaging Spectroradiometer (MODIS) on EOS-AM1. IEEE Trans. Geosci. Remote Sens., 36, 088–1100.

Castellanos, P., da Silva, A., Darmenov, A., Buchard, V., Govindaraju, R., Ciren, P., & Kondragunta, S. (2019). A Geostationary Instrument Simulator for Aerosol Observing System Simulation Experiments. *Atmosphere*, *10*(1), 2–36. http://doi.org/10.3390/atmos10010002

Chang, I., Gao, L., Burton, S. P., Chen, H., Diamond, M. S., Ferrare, R. A., et al. (2021). Spatiotemporal heterogeneity of aerosol and cloud properties over the southeast Atlantic: An observational analysis. Geophysical Research Letters, 48, e2020GL091469. https://doi.org/10.1029/2020GL091469

Chin, M., P. Ginoux, S. Kinne, O. Torres, B. N. Holben, B. N. Duncan, R. V. Martin, J. A. Logan, A. Higurashi, and T. Nakajima, 2002: Tropospheric Aerosol Optical Thickness from the GOCART Model and Comparisons with Satellite and Sun Photometer Measurements. J. Atmos. Sci., 59, 461–483.

da Silva, A.M., W. Putman and J. Nattala, 2014: File Specification for the 7-km GEOS-5 Nature Run, Ganymed Release (Non-hydrostatic 7-km Global Mesoscale Simulation). GMAO Office Note No. 6 (Version 1.0), 176 pp, available from http://gmao.gsfc.nasa.gov/pubs/office_notes.

Derber J.C., D.F. Parrish and S.J. Lord, 1991: The new global operational analysis system at the National Meteorological Center. Weath. Forec. 6, 538-547.

Devasthale, A., and M. A. Thomas 2011: A global survey of aerosol-liquid water cloud overlap based on four years of CALIPSO-CALIOP data. Atmos. Chem. Phys., 11, 1143–1154, doi:10.5194/acp-11-1143-2011

Gelaro, R., W. Putman, S. Pawson, C. Draper, A. Molod, P.M. Norris, L.E. Ott, N. Prive, O. Reale, D. Achuthavarier, M. Bosilovich, V. Buchard, W. Chao, L. Coy, R. Cullather, A.M. da Silva, A. Darmenov, R.M. Errico, M. Fuentes, M.J. Kim, R. Koster, W. McCarty, J. Nattala, G. Partyka, S. Schubert, G. Vernieres, Y. Vikhliaev, K. Wargan, 2015: Evaluation of the 7-km GEOS-5 Nature Run. Technical Report. NASA/TM-2014-104606, Goddard Space Flight Center, National Aeronautics and Space Administration.

Haywood, J. M., S. R. Osborne, P. N. Francis, A. Keil, P. Formenti, M. O. Andreae, and P. H. Kaye, 2003: The mean physical and optical properties of regional haze dominated by biomass burning aerosol measured from the C-130 aircraft during SAFARI 2000, J. Geophys. Res.,108(D13), 8473, doi:10.1029/2002JD002226.

Hess, M., P. Koepke, and I. Schult, 1998: Optical properties of aerosols and clouds: The software package OPAC. B. Am. Meteorol. Soc., 79(5), 831–844.

Hill, C., C. DeLuca, V. Balaji, M. Suarez, A. da Silva, 2004: The architecture of the Earth System Modeling Framework, Comp. Sci. Engr., 6(1), 18-28.

Hoffman, R. N. and R. Atlas, 2016: Future Observing System Simulation Experiments. BAMS, 97(9), 1601–1616. http://doi.org/10.1175/BAMS-D-15-00200.1

Holben, B.N., T. F. Eck, I. Slutsker, D. Tanre, J.P. Buis, A. Setzer, E.F. Vermote, J. A.

Reagan, Y.J. Kaufman, T. Nakajima, F. Lavenu, I. Jankowiak, A. Smirnov, 1998: AERONET – A federated instrument network and data archive for aerosol characterization. Rem. Sens. Env., v.66, n1, p1-16.

Hsu, N.C., M-J. Jeong, C. Bettenhausen, A.M. Sayer, R. Hansell, C.S. Seftor, J. Huang, S-C. Tsay 2013: Enhanced Deep Blue aerosol retrieval algorithm: The second generation. J. Geophys. Res.-Atmos., 118(16), p 9296-9315.

Hubanks, P., S. Platnick, M.D. King, W. Ridgway, 2019: MODIS Level-3 daily gridded product. https://modis-atmos.gsfc.nasa.gov/images/l3-daily-browse

Jethva, H., O. Torres, F. Waquet, D. Chand, D., & Y. Hu, 2014: How do A-train sensors intercompare in the retrieval of above-cloud aerosol optical depth? A case study-based assessment. Geophysical Research Letters. http://doi.org/10.1002/(ISSN)1944-8007

Kaufman, Y. J., A. E. Wald, L. A. Remer, B. C. Gao, R. R. Li, L. Flynn, 1997: The MODIS 2.1μm channel - Correlation with visible reflectance for use in remote sensing of aerosol IEEE Trans. Geosci. Remote Sens., Vol. 35, 1286-1298.

Kim, M.-H., Omar, A. H., Tackett, J. L., Vaughan, M. A., Winker, D. M., Trepte, C. R., Hu, Y., Liu, Z., Poole, L. R., Pitts, M. C., Kar, J., and Magill, B. E.: The CALIPSO version 4 automated aerosol classification and lidar ratio selection algorithm, Atmos. Meas. Tech., 11, 6107–6135, https://doi.org/10.5194/amt-11-6107-2018, 2018.

Kratz, D.P. 1995: The correlated-k distribution technique as applied to the AVHRR channels. J. Quant. Spectrosc. Rad. Trans. 53, 501-517.

LeBlanc, S. E., Redemann, J., Flynn, C., Pistone, K., Kacenelenbogen, M., Segal-rosenheimer, M., Shinozuka, Y., Dunagan, S., Dahlgren, R. P., Meyer, K., Podolske, J., Howell, S. G., Freitag, S., Small-griswold, J., Holben, B., Diamond, M., Wood, R., Formenti, P., Piketh, S., Maggs-Kölling, G., Gerber, M. and Namwoonde, A.: Above-cloud aerosol optical depth from airborne observations in the southeast Atlantic, Atmos. Chem. Phys., 20, 1565–1590, doi:10.5194/acp-20-1565-2020, 2020.

Levy, R. C., S. Mattoo, L. A. Munchak, L. A. Remer, A. M. Sayer, F. Patadia, and N. C. Hsu, 2013: The Collection 6 MODIS aerosol products over land and ocean, Atmos. Meas. Tech., 6, 2989-3034, doi:10.5194/amt-6-2989-2013.

Levy, R.C., L. A. Remer, D. Tanre, S. Mattoo, Y.J. Kaufman, 2009: Algorithm for remote sensing of tropospheric aerosol over dark targers from MODIS Collections 005 and 051, revision 2. ATBD Reference Number: ATBD-MOD-04. http://modis-atmos.gsfc.nasa.gov/reference_atbd.html

Menzel, W. P., R. Frey, H. Zhang, D. Wylie, C. Moeller, R. Holz, B. Maddux, B. A. Baum, K. Strabala, and L. Gumley, 2008: MODIS global cloud-top pressure and amount estimation: Algorithm description and results. J. Appl. Meteor. Climatol., 47, 1175–1198.

Meyer, K. G., S. Platnick. 2015: Simultaneously inferring above-cloud absorbing aerosol optical thickness and underlying liquid phase cloud optical and microphysical properties using MODIS. *J. Geophys. Res. Atmos*, 120 (11): 5524–5547

Meyer, K. G., S. Platnick, L. Oreopoulos, and D. Lee. 2013: Estimating the direct radiative effect of absorbing aerosols overlying marine boundary layer clouds in the southeast Atlantic using MODIS and CALIOP. *J. Geophys. Res. Atmos.,* 118 (10): 4801-4815

Molod, A., L. Takacs, M. Suarez, J. Bacmeister, I.-S. Song, and A. Eichmann, 2012: The

GEOS-5 Atmospheric General Circulation Model: Mean Climate and Development from MERRA to Fortuna. Tech. Rep. S. Gl. Mod. Data Assim., 28

Moody, E. G., M. D. King, C. B. Schaaf, D. K. Hall, and S. Platnick, 2007: Northern Hemisphere five-year average (2000-2004) spectral albedos of surfaces in the presence of snow: Statistics computed from Terra MODIS land products. Remote Sens. Environ., 111, 337–345.

Moody, E. G., M. D. King, C. B. Schaaf and S. Platnick, 2008: MODIS-derived spatially complete surface albedo products: Spatial and temporal pixel distribution and zonal averages. J. Appl. Meteor. Climatol., 47, 2879–2894.

Norris, P. M., L. Oreopoulos, A. Y. Hou, W.-K. Tao, X. Zeng, 2008: Representation of 3D heterogeneous cloud fields using copulas: Theory for water clouds. J. Q. R. Meteorol. Soc. 134: 1843–1864. doi:10.1002/qj.321.

Norris, P. M., and A. M. da Silva. 2016a: Monte Carlo Bayesian inference on a statistical model of sub-gridcolumn moisture variability using high-resolution cloud observations. Part 1: Method. Q.J.R. Meteorol. Soc., 142 (699): 2505-2527.

Norris, P. M., and A. M. da Silva. 2016b: Monte Carlo Bayesian inference on a statistical model of sub-gridcolumn moisture variability using high-resolution cloud observations. Part 2: Sensitivity tests and results. Q.J.R. Meteorol. Soc., 142 (699): 2528-2540.

Notarnicola, C., D. Di Rosa, F. Posa, 2011: Cross-Comparison of MODIS and CloudSat Data as a Tool to Validate Local Cloud Cover Masks. Atmos., 2, 242-255, doi:10.3390/atmos2030242

Pincus, R., S. Platnick, S. A. Ackerman, R. S. Hemler, and R. J. P. Hofmann, 2012: Reconciling simulated and observed views of clouds: MODIS, ISCCP, and the limits of instrument simulators. J. Climate, 25, 4699-4720. doi:10.1175/JCLI-D-11-00267.1.

Pistone, K., Redemann, J., Doherty, S., Zuidema, P., Burton, S., Cairns, B., Cochrane, S., Ferrare, R., Flynn, C., Freitag, S., Howell, S. G., Kacenelenbogen, M., LeBlanc, S., Liu, X., Schmidt, K. S., III, A. J. S., Segal-Rozenhaimer, M., Shinozuka, Y., Stamnes, S., van Diedenhoven, B., Van Harten, G. and Xu, F.: Intercomparison of biomass burning aerosol optical properties from in situ and remote-sensing instruments in ORACLES-2016, Atmos. Chem. Phys., 19, 9181–9208, doi:10.5194/acp-19-9181-2019, 2019.

Platnick, S., K.G. Meyer, M.D. King, G. Wind, N. Amarasinghe, B. Marchant, G.T. Arnold, Z. Zhang, P.A. Hubanks, R.E. Holz, P. Yang, W. Ridgway and J. Riedi, 2017: The MODIS Cloud Optical and Microphysical Products: Collection 6 Updates and Examples from Terra and Aqua. IEEE Trans. Geo. Rem. Sens. 55(1), 502-525, doi:10.1109/TGRS.2016.2610522

Platnick, S., K.G. Meyer, N. Amarasinghe, G. Wind, P.A. Hubanks and R.E. Holz 2020: Sensitivity of Multispectral Imager Liquid Water Cloud Microphysical Retrievals to the Index of Refraction. Rem. Sens. 2020, 12, 4165; doi:10.3390/rs12244165

Putman W., A.M. da Silva, L.E. Ott and A. Darmenov, 2014: Model Configuration for the 7-km GEOS-5 Nature Run, Ganymed Release (Non-hydrostatic 7 km Global Mesoscale Simulation). GMAO Office Note No. 5 (Version 1.0), 18 pp, available from http://gmao.gsfc.nasa.gov/pubs/office_notes.

Randles, C. A., A.M. da Silva, and V Buchard, 2017: The MERRA-2 Aerosol Reanalysis, 1980–onward, Part I: System Description and Data Assimilation Evaluation. *Journal of Climate*. http://doi.org/10.1175/JCLI-D-16-0609.s1

604

Redemann, J., Wood, R., Zuidema, P., Doherty, S. J., Luna, B., LeBlanc, S. E., Diamond, M. S., Shinozuka, Y., Chang, I. Y., Ueyama, R., Pfister, L., Ryoo, J.-M., Dobracki, A. N., da Silva, A. M., Longo, K. M., Kacenelenbogen, M. S., Flynn, C. J., Pistone, K., Knox, N. M., Piketh, S. J., Haywood, J. M., Formenti, P., Mallet, M., Stier, P., Ackerman, A. S., Bauer, S. E., Fridlind, A. M., Carmichael, G. R., Saide, P. E., Ferrada, G. A., Howell, S. G., Freitag, S., Cairns, B., Holben, B. N., Knobelspiesse, K. D., Tanelli, S., L'Ecuyer, T. S., Dzambo, A. M., Sy, O. O., McFarquhar, G. M., Poellot, M. R., Gupta, S., O'Brien, J. R., Nenes, A., Kacarab, M., Wong, J. P. S., Small-Griswold, J. D., Thornhill, K. L., Noone, D., Podolske, J. R., Schmidt, K. S., Pilewskie, P., Chen, H., Cochrane, S. P., Sedlacek, A. J., Lang, T. J., Stith, E., Segal-Rozenhaimer, M., Ferrare, R. A., Burton, S. P., Hostetler, C. A., Diner, D. J., Seidel, F. C., Platnick, S. E., Myers, J. S., Meyer, K. G., Spangenberg, D. A., Maring, H., and Gao, L.: An overview of the ORACLES (ObseRvations of Aerosols above CLouds and their intEractionS) project: aerosol–cloud–radiation interactions in the southeast Atlantic basin, Atmos. Chem. Phys., 21, 1507–1563, https://doi.org/10.5194/acp-21-1507-2021, 2021.

Reid, J. S., et al., 2009: Global monitoring and forecasting of biomass-burning smoke: Description of and lessons from the Fire Locating and Modeling of Burning Emissions (FLAMBE) program, IEEE J. Sel. Top. Appl. Earth Obs. Remote Sens., 2, 144–162, doi:10.1109/JSTARS.2009.2027443.

Rienecker, M.M., M. J. Suarez, R. Todling, J. Bacmeister, L. Takacs, H.-C. Liu, W. Gu, M. Sienkiewicz, R. D. Koster, R. Gelaro, I. Stajner, and J. E. Nielsen, 2008: The GEOS-5 Data Assimilation System - Documentation of Versions 5.0.1, 5.1.0, and 5.2.0. Tech. Rep. S. Gl. Mod. Data Assim., 27

Rodgers, C. D. (1976), Retrieval of atmospheric temperature and composition from remote measurements of thermal radiation, Rev. Geophys. Space Phys., 14, 609–624.

Shinozuka, Y., Kacenelenbogen, M. S., Burton, S. P., Howell, S. G., Zuidema, P., Ferrare, R. A., LeBlanc, S. E., Pistone, K., Broccardo, S., Redemann, J., Schmidt, K. S., Cochrane, S. P., Fenn, M., Freitag, S., Dobracki, A., Segal-Rosenheimer, M. and Flynn, C. J.: Daytime aerosol optical depth above low-level clouds is similar to that in adjacent clear skies at the same heights: airborne observation above the southeast Atlantic, Atmos. Chem. Phys., 20(19), 11275–11285, doi:10.5194/acp-20-11275-2020, 2020.

Swap, R., M. Garstang, S. A. Macko, P. D. Tyson, W. Maenhaut, P. Artaxo, P. Kallberg, and R. Talbot (1996), The long-range transport of southern African aerosols to the tropical South Atlantic, J. Geophys. Res., 101, 23,777–23,791, doi:10.1029/95JD01049.

van der Werf, G. R., et al., 2010: Global fire emissions and the contribution of deforestation, savanna, forest, agriculture, and peat fires (1997–2009), Atmos. Chem. Phys., 10, 11,707–11,735, doi:10.5194/acp-10-11707-2010.

Wind, G., A.M. da Silva, P. M. Norris, and S. Platnick, 2013: Multi-sensor cloud retrieval simulator and remote sensing from model parameters – Part 1: Synthetic sensor radiance formulation, Geosci. Model Dev., 6, 2049-2062, doi:10.5194/gmd-6-2049-2013.

Wind, G., A.M. da Silva, P.M. Norris, S. Platnick, S. Mattoo and R. C. Levy, 2016: Multi-sensor cloud retrieval simulator and remote sensing from model parameters – Part 2: Aerosols, Geosci. Model Dev., 9, 2377-2389, doi:10.5194/gmd-9-2377-2016.

Zhang, Z., and S. Platnick, 2011: An assessment of differences between cloud effective

649   particle radius for marine water clouds from three MODIS spectral bands. J. Geophys.
650   Res., 116, D20215, doi:10.1029/2011JD016216.

651
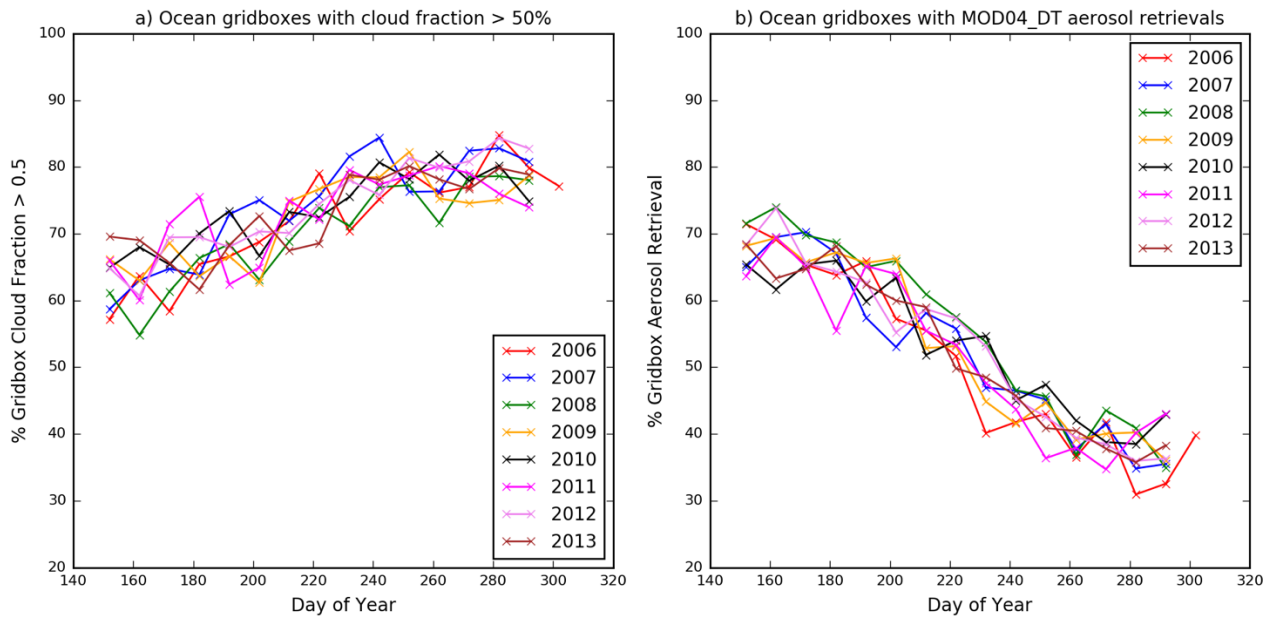
652
653 Figure 1. Terra MODIS Level-3 Daily 1-degree gridded product for SEAO area for years
654 2006-2013. Panel a) shows the percentage of SEAO ocean gridboxes that had cloud fraction
655 greater than 50%. Panel b) shows the percentage of SEAO ocean gridboxes that had any
656 successful MOD04DT aerosol property retrievals of any quality.
657
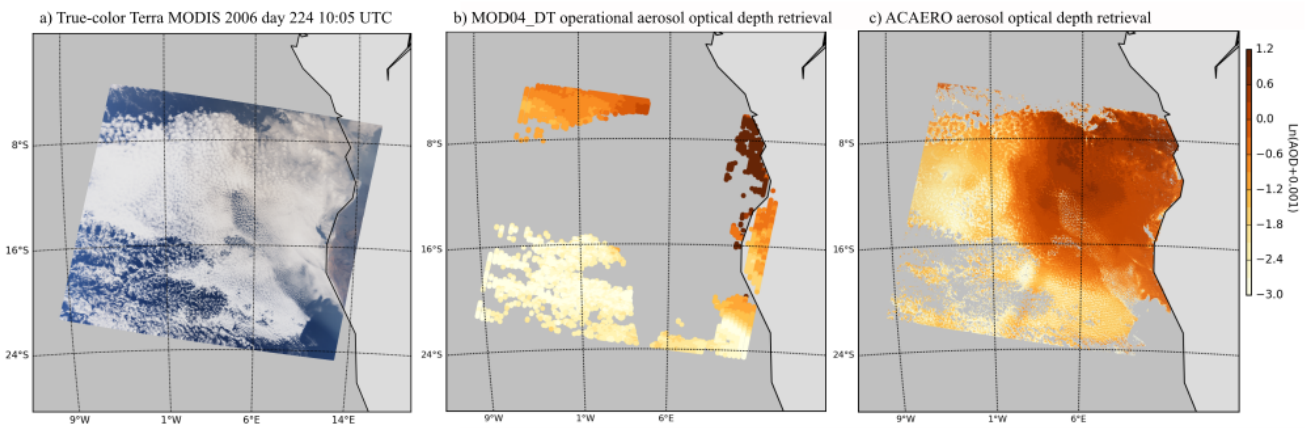
662   Figure 2. Real-data example of MOD06ACAERO retrieval. Terra MODIS 2006 day 224
663   10:05 UTC. Panel a) shows the true-color MODIS granule. There is extensive aerosol layer
664   above the equally extensive MBL cloud layer. Panel b) shows the MODIS Data Collection 6
665   operational Dark Target aerosol retrieval. It is a 10km resolution product with retrievals
666   available only in clear sky conditions and outside glint. Panel c) shows the MOD06ACAERO
667   above-cloud aerosol retrieval that is able to fill the data gap created by presence of MBL
668   layer.

a) MCARS study cases with aerosols included

MCARS T2006.224 10:05 UTC

MCARS A2006.224 12:55 UTC

MCARS T2006.225 09:10 UTC

MCARS A2006.226 12:40 UTC

MCARS T2006.228 09:40 UTC

b) MCARS study cases with aerosols removed

MCARS T2006.224 10:05 UTC

MCARS A2006.224 12:55 UTC

MCARS T2006.225 09:10 UTC

MCARS A2006.226 12:40 UTC

MCARS T2006.228 09:40 UTC
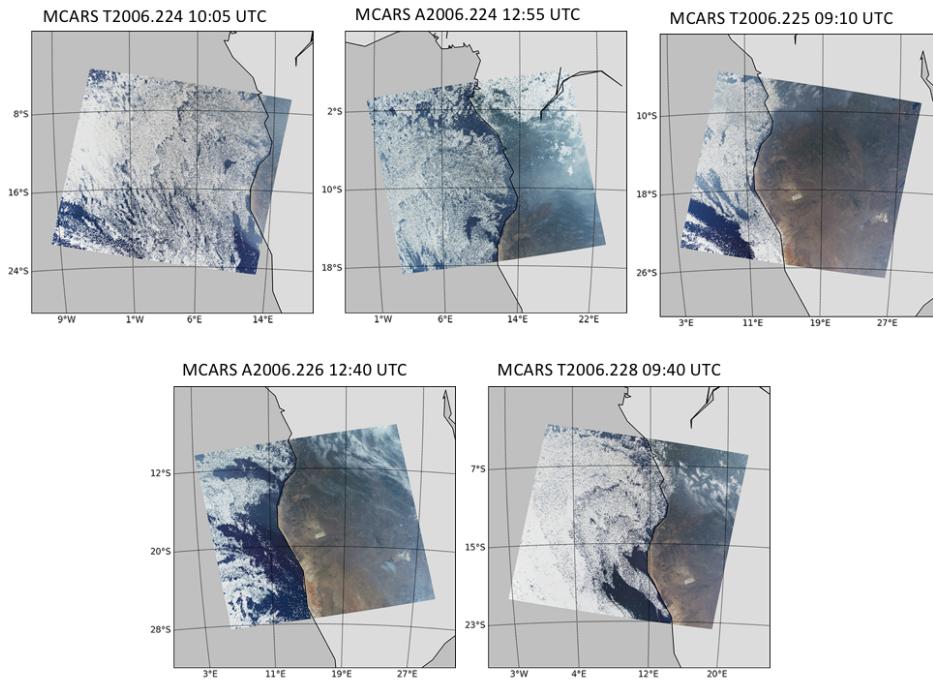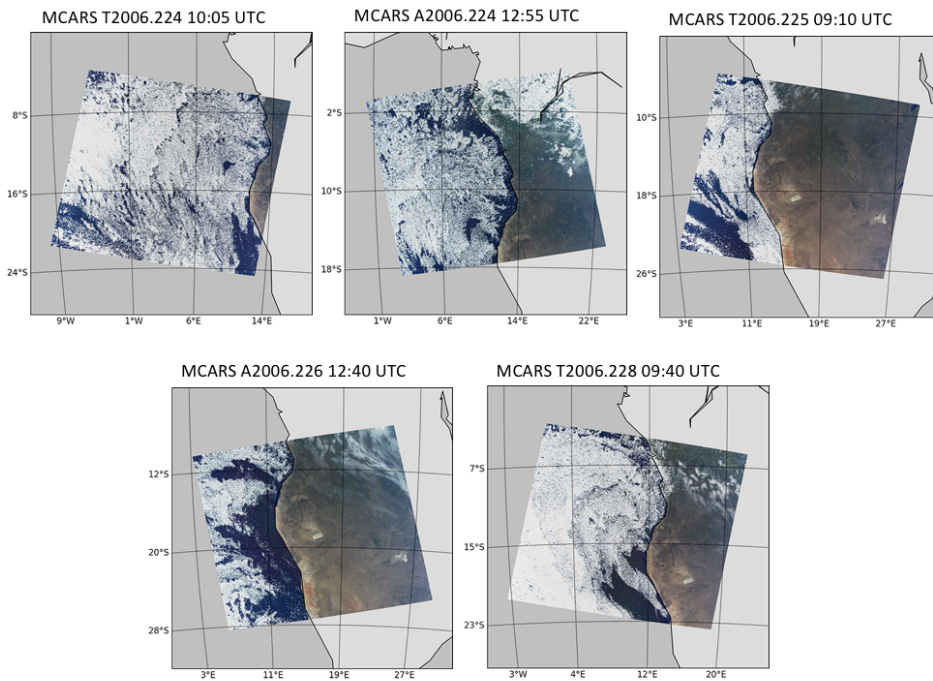
671
672 Figure 3. Scenes generated by MCARS from G5NR used in analysis of the MOD06ACAERO
673 product. There are three cases based on Terra MODIS, designated with a T next to the year.
674 There are two cases based on Aqua MODIS, designated with an A next to the year. Panel a)
675 shows the case set simulated with aerosols present. Panel b) shows the same case set but
676 simulated with aerosols removed.
677
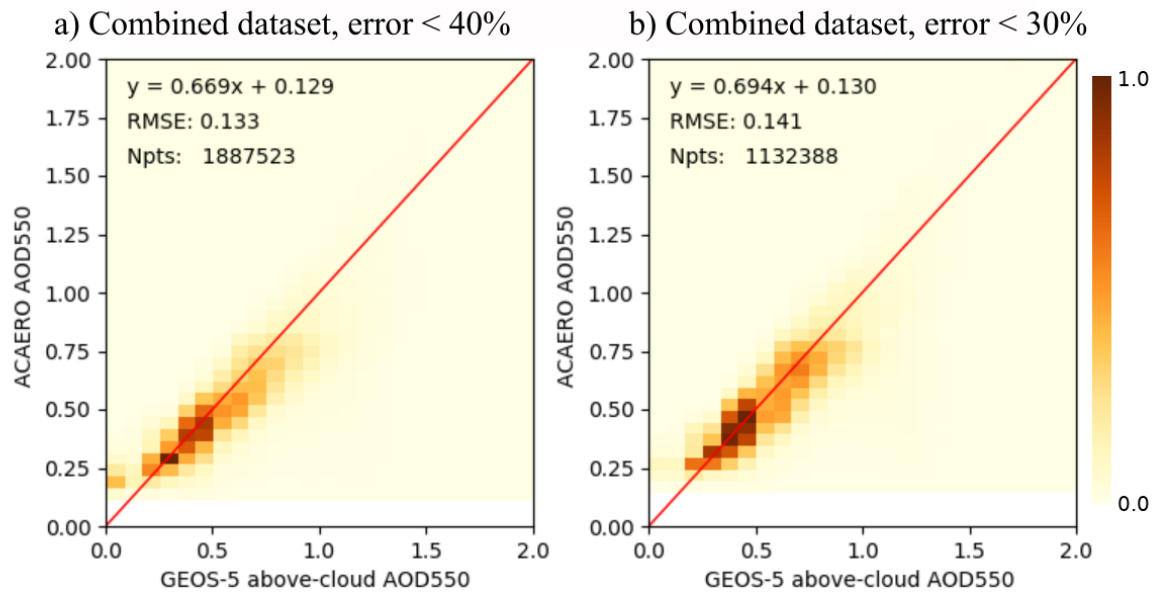
Figure 4. MOD06ACAERO retrieval results from the combined dataset of Figure 3a compared to source GEOS-5 aerosol optical depth as a normalized density plot. No screening of retrievals had been performed except for pixel-level uncertainty. Panel a) shows MOD06ACAERO retrievals with uncertainty of less than 40% and panel b) shows same with uncertainty less than 30%.
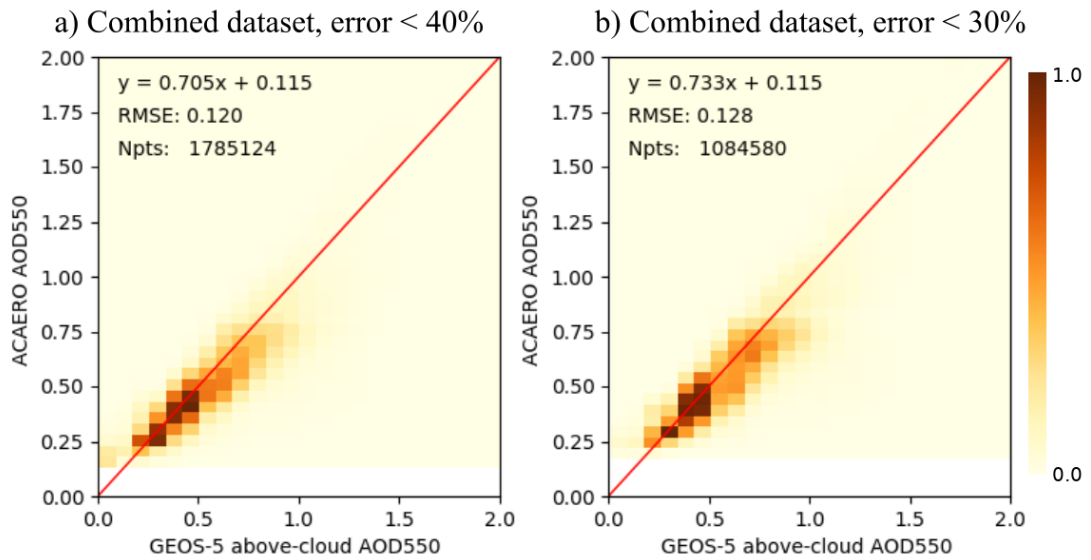
Figure 5. MOD06ACAERO retrieval results from the combined dataset of Figure 3a compared to source GEOS-5 aerosol optical depth as a normalized density plot. AOD retrievals where COT was less than 4 are now discarded. Panel a) shows MOD06ACAERO retrievals with uncertainty of less than 40% and panel b) shows same with uncertainty less than 30%.
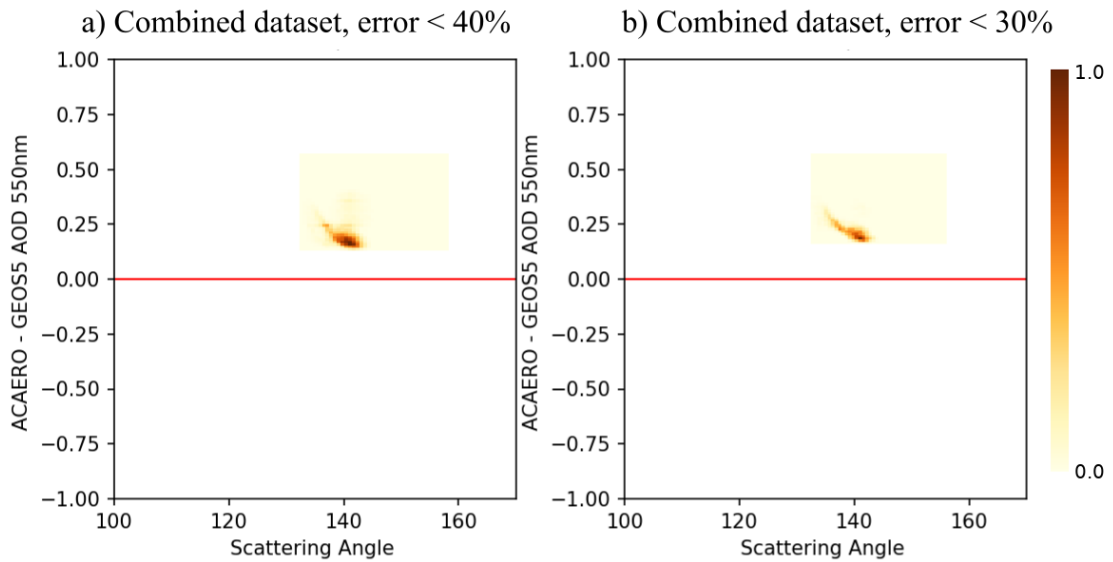
693
694 Figure 6. MOD06ACAERO retrieval results from the combined dataset of Figure 3b, where
695 aerosols had been removed. The results are displayed as difference from GEOS-5 AOD,
696 which in this case was zero, as a function of scattering angle as a normalized density plot. All
697 retrievals where MOD06ACAERO result was also zero had been removed for clarity. All
698 non-zero MOD06ACAERO retrievals appear to be concentrated in a narrow angle range
699 between 135 and 145 degrees which corresponds to the cloud bow. Panel a) shows
700 MOD06ACAERO retrievals with uncertainty of less than 40% and panel b) shows same with
701 uncertainty less than 30%.
702
703
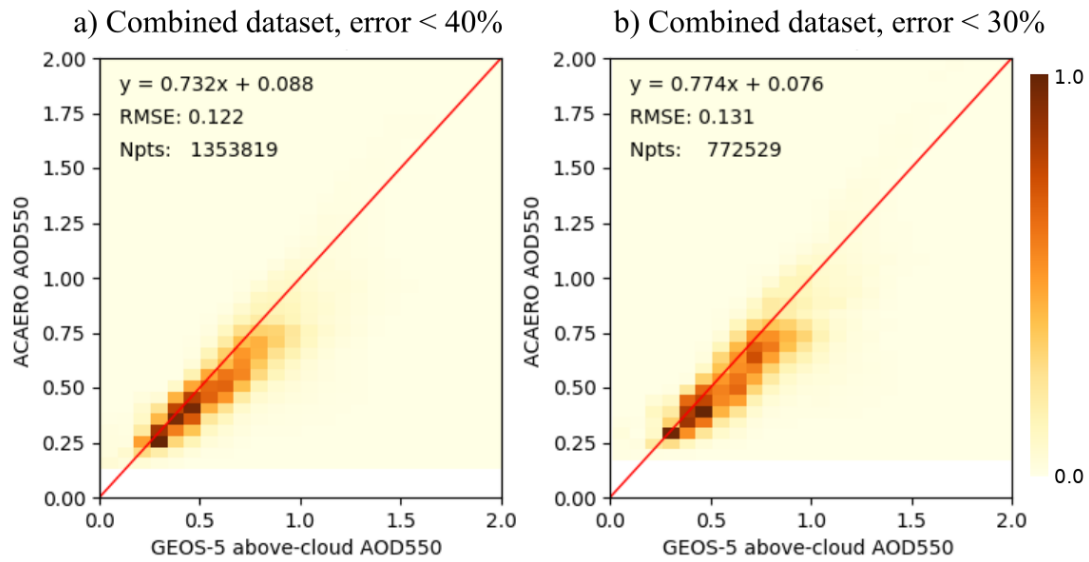
704
705 Figure 7. MOD06ACAERO retrieval results from the combined dataset of Figure 3a
706 compared to source GEOS-5 aerosol optical depth as a normalized density plot. AOD
707 retrievals where COT was less than 4 are now discarded. Additionally retrievals in the cloud
708 bow region are also removed. It appears they were indeed the source of a cluster of higher
709 MOD06ACAERO retrievals when GEOS-5 AOD was near zero and the match up with
710 GEOS-5 source AOD is further improved. Panel a) shows MOD06ACAERO retrievals with
711 uncertainty of less than 40% and panel b) shows same with uncertainty less than 30%.
712
713
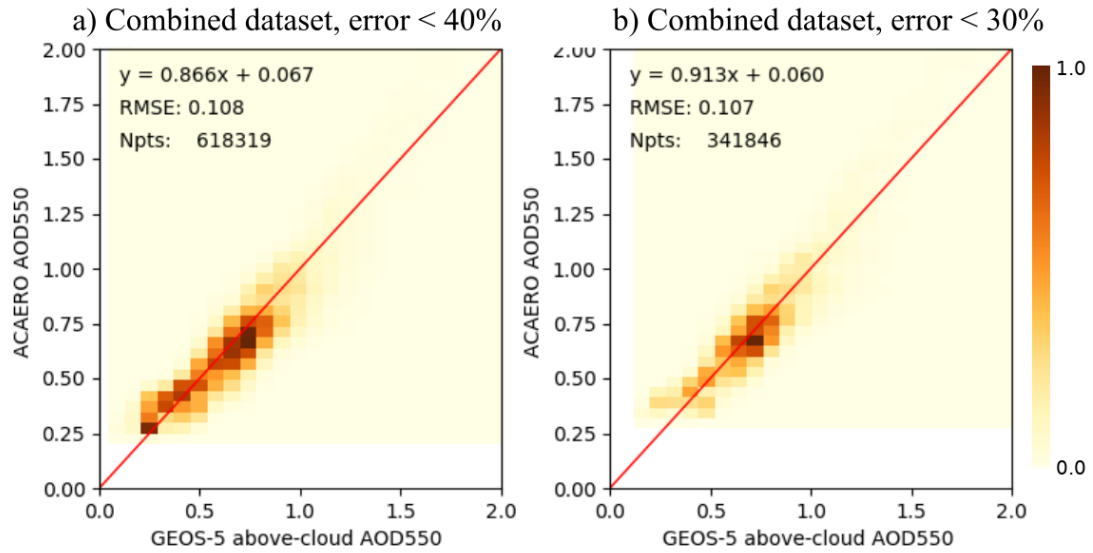
714
715 Figure 8. MOD06ACAERO retrieval results from the combined dataset of Figure 3a
716 compared to source GEOS-5 aerosol optical depth as a normalized density plot. AOD
717 retrievals where COT was less than 4 and where the scattering angle was in the cloud bow are
718 now discarded. Additionally the data extent had been limited to only include pixels with view
719 zenith angle of less than 32 degrees. Retrieval comparison shows further improvement. Panel
720 a) shows MOD06ACAERO retrievals with uncertainty of less than 40% and panel b) shows
721 same with uncertainty less than 30%.
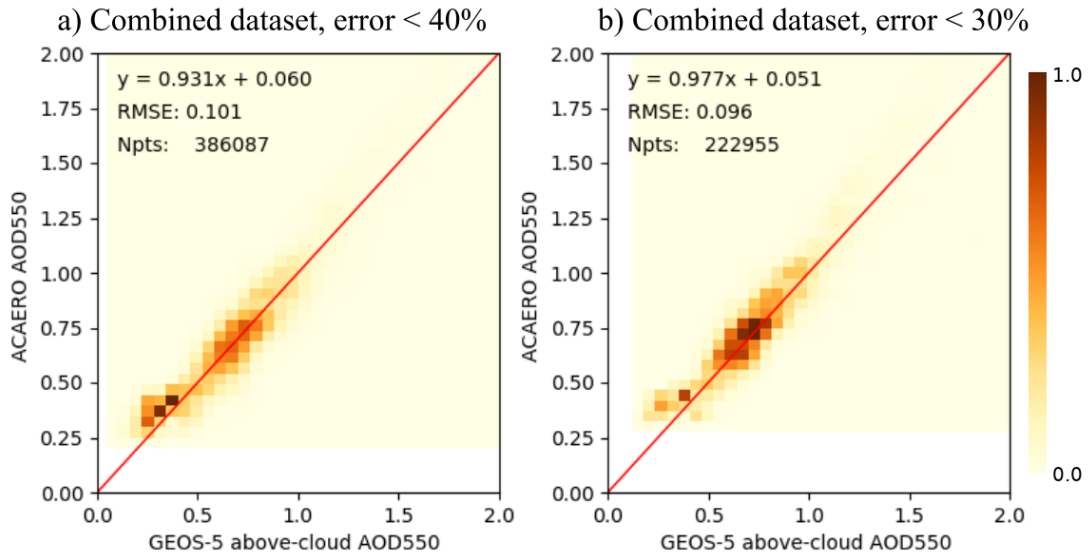
722
723 Figure 9. MOD06ACAERO retrieval results from the combined dataset of Figure 3a
724 compared to source GEOS-5 aerosol optical depth as a normalized density plot. AOD
725 retrievals where COT was less than 4 and where the scattering angle was in the cloud bow are
726 now discarded. Additionally the data extent had been limited to only include pixels with view
727 zenith angle of less than 20 degrees. Retrieval comparison shows further improvement
728 however it is not clear if the reduction in dataset size is worth the gain in accuracy. Panel a)
729 shows MOD06ACAERO retrievals with uncertainty of less than 40% and panel b) shows
730 same with uncertainty less than 30%.
731
732
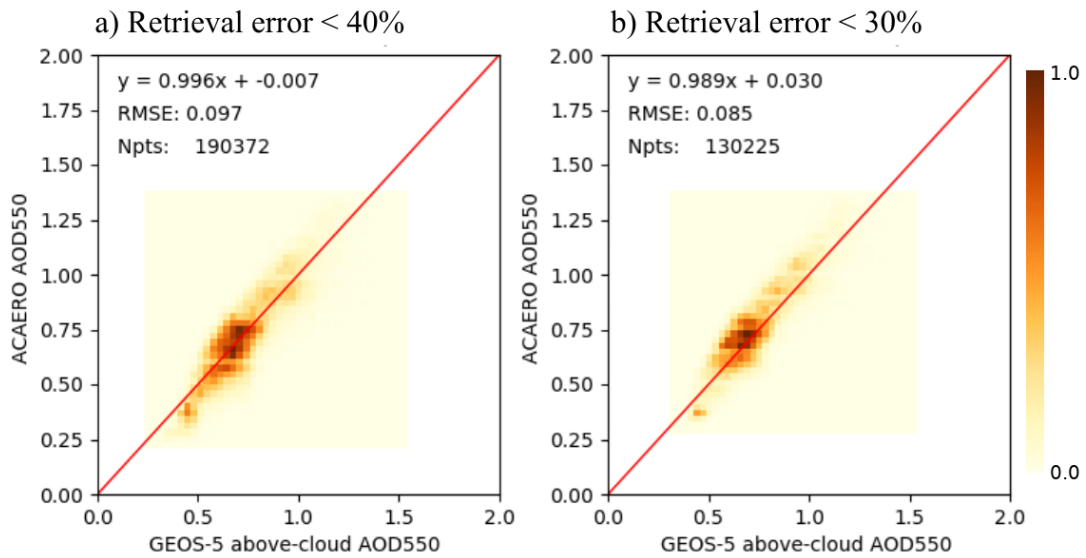
733
734   Figure 10. MOD06ACAERO retrieval results from simulated MCARS granule based on Terra
735   MODIS 2006 day 224 10:05 UTC compared to source GEOS-5 aerosol optical depth as a
736   normalized density plot. In this experiment both MOD06 and MOD06ACAERO were
737   modified to use MCARS pixel-level atmospheric profiles to perform atmospheric correction.
738   AOD retrievals where COT was less than 4 and where the scattering angle was in the cloud
739   bow are now discarded. Additionally the data extent had been limited to only include pixels
740   with view zenith angle of less than 20 degrees. This experiment shows excellent agreement
741   with source data. Panel a) shows MOD06ACAERO retrievals with uncertainty of less than
742   40% and panel b) shows same with uncertainty less than 30%. The small dataset size in panel
743   b) is the reason for slightly lower agreement with source compared to panel a)
744